Ultraviolet transmission spectroscopy of the transiting exoplanet WASP-12b

L. Fossati[1], C. A. Haswell[1], C. Froning[2], and co-authors in Fossati et al. 2010a

[1]Department of Physics and Astronomy, Open University, Walton Hall, Milton Keynes MK7 6AA, UK; [2]Center for Astrophysics and Space Astronomy, University of Colorado, 593 UCB, Boulder, CO 80309-0593, USA

Introduction and Observations

Observations of the transiting extrasolar planets HD209458b and HD189733b revealed an enhanced transit depth at the wavelengths of several UV resonance lines (Vidal-Madjar et al. 2003, 2004, Lecavelier des Etangs et al. 2010). These UV lines from the ground state are sensitive probes of the presence of atomic and ionic species. Their presence enhanced the effective radius of the planet during transit, implying the planet is surrounded by an extended cloud of size comparable to or larger than its Roche lobe (Vidal-Madjar et al. 2003, 2004, 2008, Ben-Jaffel 2007). WASP-12b is one of the hottest and most irradiated transiting exoplanets and orbits extremely close to a late F-type host star (Hebb et al. 2009, Fossati et al. 2010b). WASP-12b is, therefore, an attractive target to explore the properties of the exospheric cloud surrounding the planet.

The initial UV observations of HD209458b were in the far UV around the Ly α emission line. The large hydrogen abundance makes this an attractive line to observe, but the temporal and spatial variability of stellar Ly α emission is a highly undesirable complicating factor, as Fig. 1 shows. For this reason, and to obtain better signal to noise, we observed WASP-12 in the near UV where there are several resonance lines (Morton 1991, 2000), including the very strong Mg II UV resonance lines. This work became possible with the installation of the Cosmic Origins Spectrograph (COS) on the Hubble Space Telescope (HST).

HST observed WASP-12 for five consecutive orbits on 2009 September 24th and 25th with COS (Green et al. 2010, Osterman et al. 2010). We used the NUV G285M grating at the 2676 Å setting, which provides non-contiguous spectra over three wavelength ranges (NUVA: 2539–2580 Å, NUVB: 2655–2696 Å, and NUVC: 2770–2811 Å; the three observed spectral ranges are shown from top to bottom in Fig. 1) at a spectral resolution of $R \sim$20 000, in TIME-TAG mode, with an exposure time of about 2334 sec in the first HST orbit and about 3000 sec per subsequent HST orbit. The data reduction was performed with CALCOS V.2.11b, adopting the most up-to-date set of reference files, that, despite the early date of our observations, were at a fairly mature stage. In particular, the flat field had been updated to its flight version.

In our time series analysis we used the count rates obtained after background subtraction, rather than the flux calibrated spectra. The high quality flat-field and the relatively low background of the NUV channel, mean the uncertainties are dominated by poisson statistics. The resulting signal to noise ratio (SNR) per pixel in the NUVB spectrum is ∼10 for each 3000 sec exposure.

Figure 1 shows the total summed spectrum in comparison with synthetic fluxes from the LLMODELS stellar model atmosphere code (Shulyak et al. 2004), assuming the fundamental parameters and abundances given by Fossati et al. 2010b. All three regions are strongly affected by many blended photospheric features. The NUVB region is closest to the continuum, while the NUVC region is strongly absorbed by the Mg II doublet at 2795.5 Å and 2802.7 Å, and does not show any emission feature in the line cores. This might be connected with an unusual stellar activity and more details can be found in Fossati et al. (2010b) and Haswell et al (2010).

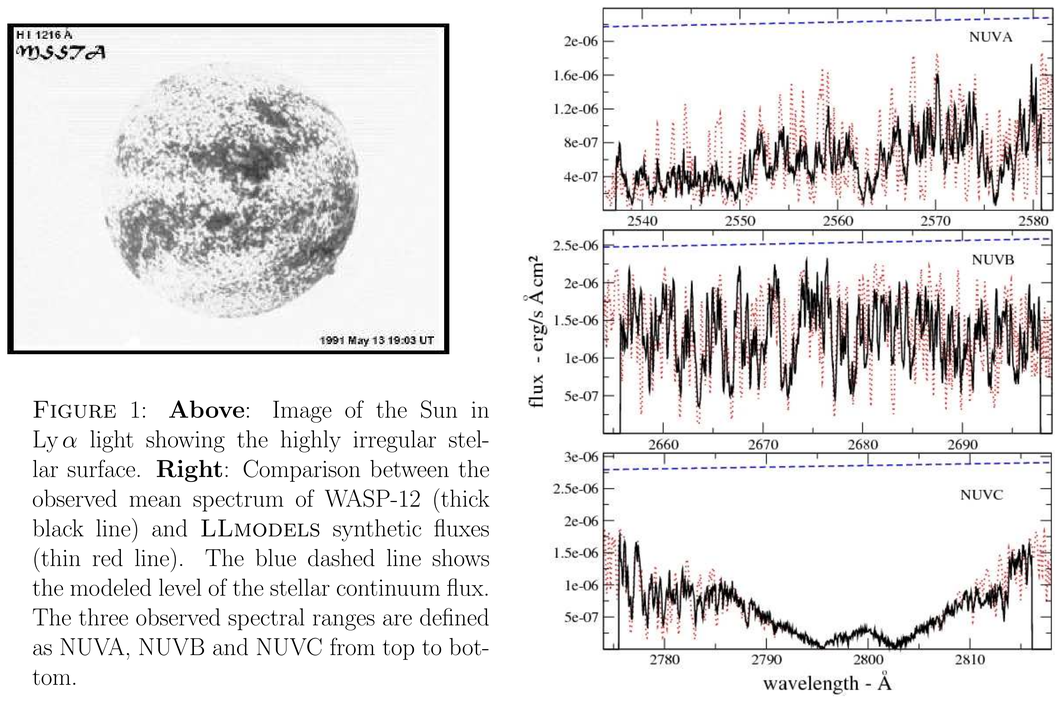

FIGURE 1: **Above**: Image of the Sun in Ly α light showing the highly irregular stellar surface. **Right**: Comparison between the observed mean spectrum of WASP-12 (thick black line) and LLMODELS synthetic fluxes (thin red line). The blue dashed line shows the modeled level of the stellar continuum flux. The three observed spectral ranges are defined as NUVA, NUVB and NUVC from top to bottom.

The near UV transit light curve

Figure 2 shows the comparison between the light curves obtained for each observed wavelength range and the one calculated from visible photometry. The NUVB wavelength range is the closest to the continuum and shows a transit depth that matches, at $\sim 1\sigma$, the transit light curve derived by Hebb et al. (2009) from optical photometry. In the NUVA and NUVC wavelength ranges we obtained a deeper transit at about 2.5σ level. These three light curves were normalised to the line passing through the out-of-transit photometric points (first and fifth exposures). The slope of the three normalisation lines are 3.8×10^{-3} for the NUVA region, 3.3×10^{-2} for the NUVB region, and 1.0×10^{-2} for the NUVC region. These values are small enough that the applied normalisation did not change the transit shape.

The NUVC spectral region is clearly dominated by the Mg II resonance lines that are likely to be responsible for the detected extra depth in the transit light curve. The NUVA spectral region includes resonance lines of Na I, Al I, Sc II, Mn II, Fe I, and Co I (Morton 1991, 2000). The stellar spectrum is dominated by Mg I and Fe I lines coming from low energy levels. Given the high exospheric temperature, it is likely that these spectral features might be present also in the spectrum of the planet atmosphere, and that therefore are responsible for the observed deeper transit.

The end of the second exposure is at the phase of the planet ingress, as shown in Fig. 2. It is notable that the NUVA flux during the second exposure lies below the out-of-transit level by $\sim 2\sigma$. We divided this particular exposure into three equal sub-exposures plotted as black crosses. These suggest an early ingress in the NUVA spectral region. We treated the other exposures in the same way, but found no trends in them. The early ingress phenomenon has been recently theoretically explained by Lai et al. (2010).

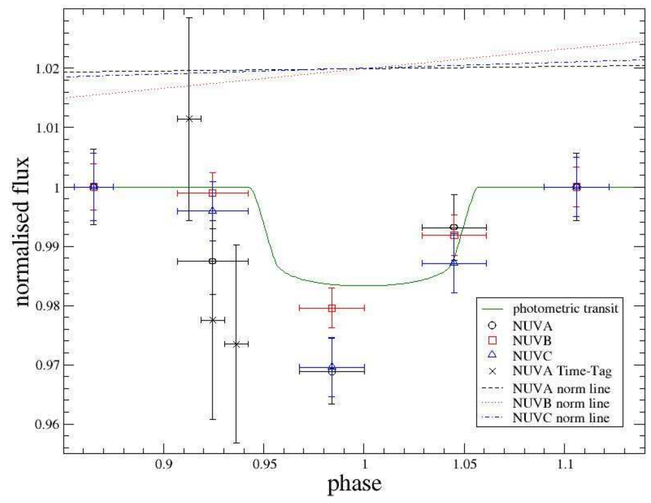

FIGURE 2: Light curve obtained for each observed wavelength range (NUVA: open black circles - NUVB: open red squares - NUVC: open blue triangles). The horizontal error bar defines the orbital phase range covered by each observation. The vertical uncertainty comes from a Poissonian treatment of the error bars. The full green line shows the MCMC fit to the optical transit light curve (Hebb et al. 2009). The black crosses show the NUVA spectral range split into three equally exposed sub-exposures. Lines indicate the normalisation gradients applied.

The transit depths in the NUVA, NUVB, and NUVC wavelength ranges respectively imply effective planet radii of 2.69±0.24 R_J, 2.18±0.18 R_J, and 2.66±0.22 R_J. WASP-12b's optical radius is $R_P = 1.79 \pm 0.09\, R_J$ while the mean Roche lobe radius is 2.36 R_J using Paczyński's (1971) prescription. This leads to the conclusion that WASP-12b is surrounded by an exosphere which over-fills the planet's Roche lobe, confirming predictions by Li et al. (2010).

The Mg II detection

In each of the three wavelength ranges we calculated a ratio spectrum between the in-transit and the out-of-transit spectrum. To this ratio spectrum we associated two different uncertainties: (i) the standard deviation from the mean, which we denote σ_{exp}, and (ii) the uncertainty from the standard error propagation, which we denote σ_{prop}.

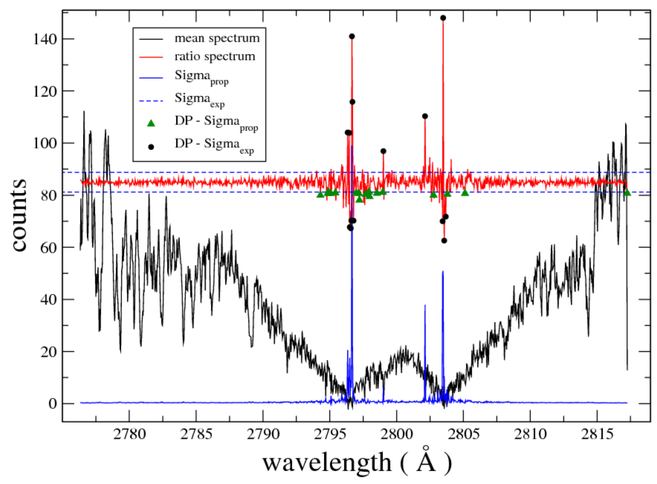

FIGURE 3: The black line shows the observed spectrum obtained averaging the five available COS spectra. The red line shows the ratio spectrum, magnified five times and shifted upwards. The blue lines show the σ_{prop} spectrum (full line) and the values of σ_{exp} (dashed lines). The full black circles show the position of the deviating points assuming $\sigma = \sigma_{exp}$, while the full green triangles show the position of the deviating points assuming $\sigma = \sigma_{prop}$.

Figure 3 shows these spectra and the wavelength points that deviate more than 3σ from the mean in the NUVC wavelength region. With $\sigma = \sigma_{exp}$ the deviating points correspond to the core of the Mg II line where the signal level is low. This is to be expected since here the low count rates imply a very noisy ratio spectrum. In contrast, with $\sigma = \sigma_{prop}$ each element of the ratio spectrum is assessed against its own Poisson error. In this case the deviating points are all below the mean rate spectrum, and the deviating points appear at the margins of the line cores. These points indicate excess Mg II absorption during transit, attributable to absorption by the planet's atmosphere.

In addition, Fossati et al. (2010a) and Haswell et al. (2010) show that the planet exosphere is composed by a number of heavy elements/ions, such as Mg and Fe. WASP-12b is extremely close to the host star and consequently the stellar irradiation and tidal effects could induce prodigious mixing (possibly involving also the rocky planet surface), affecting the chemistry of the planet atmosphere, although it might also be possible that most of the elements detected in the planet exosphere belong to the stellar wind.

References

[1] Ben-Jaffel, L. 2007, ApJ, 671, L61
[2] Fossati, L., Haswell, C. A., Froning, C., et al. 2010a, ApJ, 714L, 222
[3] Fossati, L., Bagnulo, S., Elmasli, A., et al. 2010b, ApJ, 720, 872
[4] Green, J. C., et al. 2010, BAAS, 41, 501
[5] Haswell, C. A., Fossati, L., Froning, C., 2010, in prep
[6] Hebb, L., Collier-Cameron, A., Loeillet, B. et al. 2009, ApJ, 693, 1920
[7] Lecavelier des Etangs, A., Ehrenreich, D., Vidal-Madjar, A., et al. 2010, A&A, 514, 72
[8] Li, S., Miller, N., Lin, D. N. C., & Fortney, J. J. 2010, Nature, 463, 1054
[9] Lai, D., Helling, C., & van den Heuvel, E. P. J. 2010, ApJ, accepted, (arXiv: 1005.4497)
[10] Morton, D. C. 1991, ApJS, 77, 119
[11] Morton, D. C. 2000, ApJS, 130, 403
[12] Osterman, S., et al. 2010, BAAS, 41, 502
[13] Paczyński, B. 1971, ARA&A, 9, 183
[14] Shulyak, D., Tsymbal, V., Ryabchikova, T., Stütz, Ch., & Weiss, W. W. 2004, A&A, 428, 993
[15] Vidal-Madjar, A., Lecavelier des Etangs, A., Désert, J.-M., et al. 2003, Nature, 422, 143
[16] Vidal-Madjar, A., Désert, J.-M., Lecavelier des Etangs, A., et al. 2004, ApJ, 604L, 69
[17] Vidal-Madjar, A., Lecavelier des Etangs, A., Désert, J.-M., et al. 2008, ApJL, 676, L57